ACS APPLIED MATERIALS & INTERFACES

Research Article

www.acsami.org

Fabrication of 3D Hierarchical MoS_2/Polyaniline and MoS_2/C Architectures for Lithium-Ion Battery Applications

Lianren Hu, Yumei Ren, Hongxia Yang, and Qun Xu*

College of Materials Science and Engineering, Zhengzhou University, Zhengzhou 450052, P.R. China

Supporting Information

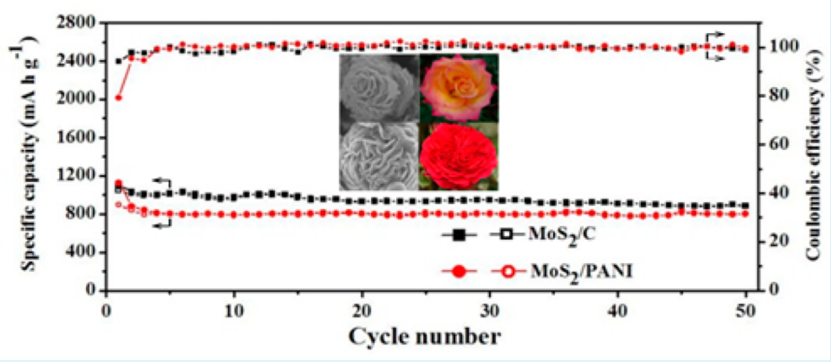

ABSTRACT: In this work, three-dimensional (3D) hierarchical MoS_2/polyaniline (PANI) nanoflowers were successfully fabricated via a simple hydrothermal method. The crystal structure and morphology of the MoS_2/PANI nanoflowers were characterized by SEM, TEM, XRD, XPS, and FT-IR spectra, revealing that the nanoflowers were composed of ultrathin nanoplates which consisted of few-layered MoS_2 nanosheets with enlarged interlayer distance of the (002) plane and PANI. The excellent electrochemical performance of the 3D hierarchical MoS_2/PANI nanoflowers was demonstrated. Further 3D hierarchical MoS_2/C nanoflowers can be prepared conveniently by annealing the MoS_2/PANI sample in a N_2 atmosphere at 500 °C for 4 h. The obtained MoS_2/C sample exhibited more excellent electrochemical performance due to its excellent electronic conductivity resulting from the close integration of MoS_2 nanosheets with carbon matrix. High reversible capacity of 888.1 mAh g^{-1} with the Coulombic efficiency maintained at above 90% from the first cycle were achieved at a current density of 100 mA g^{-1}. Even at a current density of 1000 mA g^{-1}, the reversible capacity of the MoS_2/C sample could be retained at 511 mAh g^{-1}. The excellent electrochemical performance of these two samples could be attributed to the combined action of enlarged interlayer distance of the ultrathin MoS_2 nanosheets, 3D architectures, hierarchical structures, and conductive material. Thus, these 3D hierarchical nanoflowers are competent as promising anode materials for high-performance lithium-ion batteries.

KEYWORDS: *MoS_2, nanoflowers, hierarchical structures, conductive material, lithium-ion batteries*

INTRODUCTION

There is currently an unprecedented demand for the development of large-scale electrical energy storage devices in response to the increasingly serious problems of worldwide pollution and energy crisis. As one of the most promising candidates, lithium-ion batteries (LIBs) have become the dominating power source for portable electronics because of their high energy density, excellent security, and long cycling life.[1−3] Graphite is typically used as the commercial anode material for LIBs. However, the relatively small theoretical capacity of 372 mA h g^{-1} limits its further application in high-performance LIBs.[4] Thus, exploring new anode materials with higher capacity and excellent cyclic stability is crucial for high-performance LIBs. Among the many alternative materials, layered transition-metal sulfides, such as SnS_2, MoS_2, and WS_2, have received great interest owing to their unique properties and high specific capacity.[5−9]

As a typical member of transition metal sulfides, molybdenum disulfide (MoS_2) has a layered structure held together by weak van der Waals forces, which is similar to graphite. The adjacent layers spacing of MoS_2 is 0.615 nm, significantly larger than that of graphite (0.335 nm).[10−12] Due to these desirable properties, MoS_2 can be easily intercalated by lithium ions without a significant increase in volume expansion.[13,14] Therefore, it can be regarded as a superior electrode material for LIBs. However, the performance of bulk MoS_2 is still unsatisfactory when used as anode materials in LIBs, suffering from rapid capacity fading because of its poor electrical/ionic conductivity and the structural destruction during lithiation-delithiation processes.[15−18] Considering the electrochemical properties of the electrode materials are closely

Received: June 21, 2014
Accepted: August 6, 2014
Published: August 6, 2014

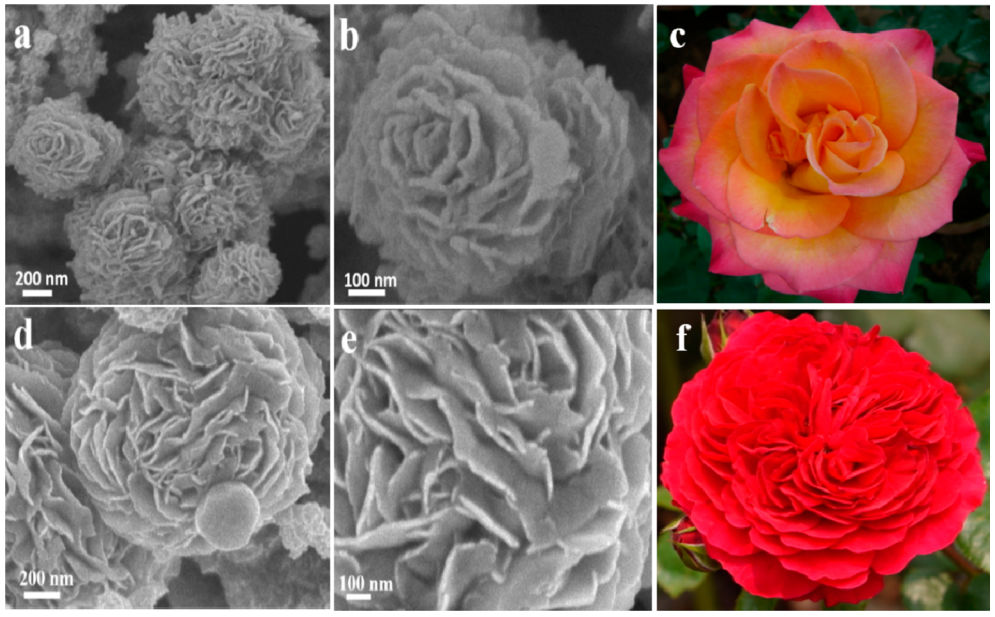

Figure 1. SEM images of the 3D hierarchical MoS_2/PANI (a, b) and MoS_2/C (d, e) nanoflowers. Photographs of two types of Chinese roses (c, f).

linked with their morphology and size, various nanostructures of MoS_2, such as nanoflowers,[19] nanoflakes,[20] nanospheres,[21] and nanosheets,[22] have been studied.

Compositing MoS_2 with conductive materials like carbon nanotubes,[17,23−27] graphene,[16,28−33] and carbon[15,34−37] to obtain uniform hybrid nanostructures is an effective approach to enhance the electrochemical performance. The conductive materials not only improve the conductance of active materials and promote rapid electron transport, but also buffer the volume expansion and stabilize the electrode structures during charge−discharge cycling. Thus, the hybrid composites can be expected to exhibit excellent electrochemical performance by making full use of the advantage of each component. For example, Lou et al. demonstrated that the MoS_2 nanosheets grown on CNTs exhibited an improved reversible capacity of 698 mA h g^{-1} at a current density of 100 mA g^{-1}.[25] Chang and Chen prepared layered MoS_2/Graphene composites by the use of L-cysteine-assisted hydrothermal process; this composite electrode could show a high reversible capacity of ∼1100 mA h g^{-1} at a current density of 100 mA g^{-1}.[28] Recently, hierarchical structures were also introduced on the basis of morphology engineering or hybridization with conductive materials to further improve the electrochemical performance. Wang et al. synthesized hierarchical hollow MoS_2 nanoparticles using a solvothermal method and found that these hollow nanoparticles exhibited remarkable enhancement in electrochemical performance compared with solid nanoparticles.[38] Yang et al. reported that one-dimensional hierarchical MoS_2/polyaniline (PANI) nanowires delivered superior electrochemical performance owing to the hierarchical and hybrid architectures.[39]

Inspired by the research above, herein we present a simple hydrothermal method to fabricate 3D hierarchical MoS_2/PANI nanoflowers using PANI as a conductive template and MoO_3, KSCN as precursors. In such hierarchical and polymer-hybrid nanoflowers, the 3D architectures ensure a large electrode−electrolyte interfacial area; the hierarchical structures provide sufficient void space which enables rapid Li ion diffusion and buffer volume expansion to some extent during the charge/discharge process; the soft and flexible chains of PANI not only improve the conductivity of the electrode material, but also enhance the structural stability. It is intersting to note that further 3D hierarchical MoS_2/C nanoflowers can also be obtained by annealing the MoS_2/PANI nanoflowers in a N_2 atmosphere at 500 °C. And more importantly, the obtained MoS_2/PANI and the MoS_2/C both exhibit high reversible capacity, and as well as good cycling stability and high-rate capability.

EXPERIMENTAL SECTION

Materials. Aniline (ANI) was purchased from Tianjin Damao Chemical Reagent Factory. Ammonium persulfate (APS), molybdic oxide (MoO_3, 99.95% purity), and potassium thiocyanate (KSCN, 99% purity) were purchased from Sigma-Aldrich. All chemicals were used as received. Electrolyte (1.0 M $LiPF_6$ dissolved in a mixture of ethylene carbonate/dimethyl carbonate/diethyl carbonate (1:1:1 v/v/v)) and lithium foil were purchased from SHENZHEN PO XON MACHINEY TECHNOLOGY CO Ltd.

Sample Preparation. Pure polyaniline (PANI) was obtained by chemical polymeration of aniline. Briefly, aniline monomers (558 mg) were added into the perchloric acid ($HClO_4$, 1 M, 199 mL) solution and sonicated for 10 min, followed by dropwise addition of $HClO_4$ solution which contained ammonium persulfate (APS, 456.4 mg). After that, a small quantity of ethanol (500 μL) was added into the solution. Then the mixture was transferred to a ice bath environment and reacted for 7 h. The obtained precipitate was washed with deionized water and ethanol several times and then dried at 60 °C under vacuum.

To synthesize 3D hierarchical MoS_2/PANI and MoS_2/C nanoflowers, the as-prepared PANI (0.1 g) was dissolved in 50 mL of deionized water with the help of ultrasonication. Then molybdic oxide (MoO_3, 0.4318 g) and potassium thiocyanate (KSCN, 0.728 g) were added into the PANI particles suspension, and the mixture was stirred for 20 min. The obtained suspension was transferred into a 50 mL Teflon-lined stainless steel autoclave and heated at 210 °C for 24 h. After cooling naturally, the black precipitate was collected by centrifugation, washed with deionized water and ethanol several times, and then dried at 60 °C for 24 h to obtain 3D hierarchical MoS_2/PANI nanoflowers. The 3D hierarchical MoS_2/PANI nanoflowers were annealed in a N_2 atmosphere at 500 °C for 4 h, while the PANI was partially carbonized to obtain the 3D hierarchical MoS_2/C nanoflowers.

Characterizations. The morphology of prepared samples was characterized by a field-emission scanning electron microscope (JEORJSM-6700F) and a transmission electron microscope (FEITecnai G2 20). The crystal structure of the prepared samples was investigated on a Y-2000 X-ray diffractometer with Cu Kα radiation (λ = 1.5406 Å) operating at 40 kV and 40 mA. X-ray photoelectron spectroscopy (XPS) measurements were performed on an ESCALABMK spectrometer using electrostatic lens mode with a pass energy of 100 eV. Fourier transform infrared (FT-IR) spectra were acquired on a TENSOR 27 FTIR spectrometer (Bruker) in the absorption mode. The Brunauer–Emmett–Teller (BET) specific surface area of the samples was determined using a Micromeritics ASAP 2020 system. The thermogravimetric analysis (TGA) measurements were conducted on a Mettler Toledo TGA/DSC 1 analyzer with a heating rate of 10 °C min^{-1} in air.

Electrochemical Measurements. The electrochemical measurements were performed using CR2032 coin cells assembled in a glovebox filled with nitrogen. The working electrode consisting of active material, carbon black and poly(vinylidene fluoride) (PVDF) at a weight ratio of 8:1:1 was prepared with the mixture of 1-meththyl-2-pyrrolidone (NMP). The resulting slurry was coated onto a copper foil which acted as a current collector, and dried at 120 °C in a vacuum overnight to remove the solvent completely, followed by pressing. A polypropylene film (Celgard-2300) was used as the separator, and lithium metal foil was used as the counter electrode. The electrolyte was 1.0 M $LiPF_6$ dissolved in a mixture of ethylene carbonate/dimethyl carbonate/diethyl carbonate (1:1:1 v/v/v). The galvanostatic charge and discharge tests were carried out on a Neware battery tester (CT-3008) with a range of 0.005–3 V at different current densities. Cyclic voltammograms (CV) were studied on a CHI 660D electrochemical workstation at a scan rate of 0.1 mV s^{-1}. The electrochemical impedance spectroscopy (EIS) tests were measured in a frequency range of 0.01 Hz to 100 kHz.

RESULTS AND DISCUSSION

Figure 1 shows the typical scanning electron microscopy (SEM) images of the 3D hierarchical MoS_2/PANI and MoS_2/C nanoflowers with different magnifications. Figure 1a demonstrates that the hierarchical flowerlike structures (shown in Figure 1c) of the MoS_2/PANI are successfully prepared. The nanoflowers have a diameter in the range of 300–700 nm, and some are independent of each other while some gather together to form clusters. The close up view shown in Figure 1b reveals that the hierarchical nanoflower consists of ultrathin nanoplates with a thickness less than 12 nm. After annealing treatment to further obtain the MoS_2/C nanoflowers, the nanoflower becomes significantly larger (Figure 1d) and the hierarchical structures become slightly denser (Figure 1e) resulting from the aggregation of the MoS_2/PANI nanoflowers during annealing process, which looks like a Red Leonardo da Vinci (Figure 1f). For both samples, the hierarchical structures provide sufficient void space between the neighboring nanoplates, which can facilitate rapid lithium diffusion and buffer the volume expansion to some extent.

The schematic illustration of the synthesis route of the 3D hierarchical MoS_2/PANI and MoS_2/C nanoflowers can be described as follows (shown in Figure 2). First, the as-prepared PANI is dispersed in deionized water with the help of ultrasonication, forming a dark green suspension (Figure S1, Supporting Information). The soft and flexible chains of PANI construct conductive networks in the suspension, on which MoS_2 can be obtained using MoO_3 and KSCN as precursors. The detail synthetic reaction of MoS_2 can be formulated as $4MoO_3 + 9SCN^- + 14H_2O \rightarrow 4MoS_2 + SO_4^{2-} + NH_4^+ + 4CO_3^{2-} + 8NH_3\ (g) + 5CO_2\ (g)$.[40] Then the nanoplates consisting of few-layered MoS_2 nanosheets and PANI assemble

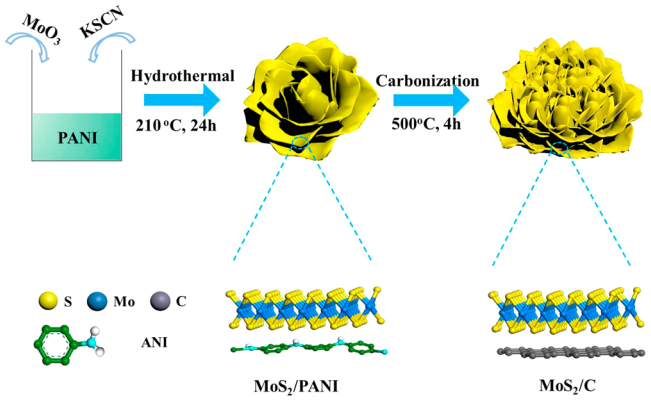

Figure 2. Schematic illustration of the preparation of 3D hierarchical MoS_2/PANI and MoS_2/C nanoflowers.

into 3D hierarchical nanoflowers during the hydrothermal process. The formation of 3D hierarchical structures is believed to be dominated mainly by the vander Waals interaction between ultrathin MoS_2 nanosheets, which has been documented in the literature.[22,41,42] Next, the MoS_2/PANI nanoflowers are annealed in a N_2 atmosphere at 500 °C for 4 h, and PANI was carbonized to further obtain the MoS_2/C sample. The morphology and chemical component of the 3D hierarchical nanoflowers are slightly different, and such variation will result in discriminating electrochemical performance.

Transmission electron microscopy (TEM) was carried out to further observe the micromorphology and structure of the nanoflowers (Figure 3). Figure 3a shows a low-magnification

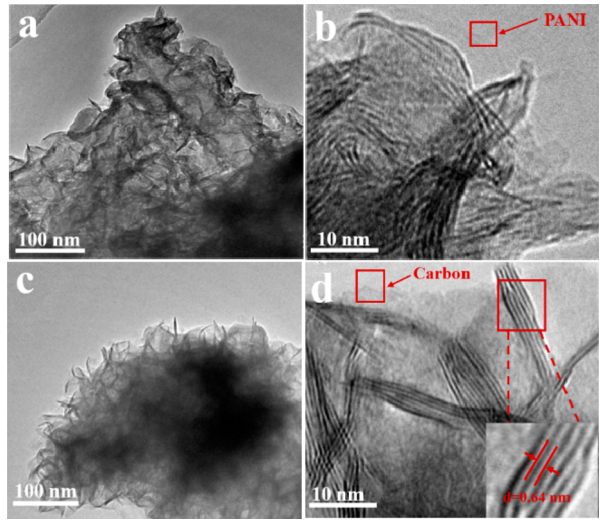

Figure 3. TEM images of the 3D hierarchical MoS_2/PANI (a, b) and the MoS_2/C (c, d) nanoflowers.

TEM image of the MoS_2/PANI sample; it can be seen that the MoS_2 nanosheets are curled and overlapped owing to their ultrathin features. A magnified TEM image in Figure 3b reveals that the MoS_2 nanosheets are dispersed on a thin PANI layer and look dark and blurred because of the poor crystallinity. After annealing treatment, the PANI was partially carbonized and the crystallinity of MoS_2 was improved. The transparency shown in Figure 3c further verifies the ultrathin dimension of the nanoplates. From the magnified TEM image of the MoS_2/C

sample in Figure 3d, the lattice fringes of MoS_2 can be clearly observed, revealing a well-defined crystal structure. The MoS_2 nanosheets consists of 2−9 layers, which are much thinner than pure MoS_2 nanosheets (Figure S2, Supporting Information), implying that the combination of PANI hinder the growth of MoS_2 crystals along the *c*-axis. In addition, the distance of the interlayer is calculated to be 0.64 nm, corresponding to the (002) plane of MoS_2, which is consistent with the following characterization of XRD result.

X-ray diffraction (XRD) measurements are used to investigate the crystal structure of the resultant materials. As shown in Figure 4, the MoS_2/PANI sample shows the same crystalline structure to the MoS_2/C sample, but a slightly lower crystallinity can be observed for the sample without being annealed. All the diffraction peaks shown in the patterns can be assigned to hexagonal MoS_2 (JCPDS 37-1492), in which the diffraction peaks at 13.8, 33, 39, 48.4, and 59.8° correspond to the (002), (100), (103), (105), and (110) planes of MoS_2, respectively.[18,22] In addition, our annealing temperature of 500 °C is much lower than the graphitization temperature of 3000 °C; the carbon in the MoS_2/C composite should be amorphous. This is why the diffraction peaks of carbon could not be observed. It is worth noting that the diffraction peak at 13.8° corresponding to the (002) plane of MoS_2 is lower than that of bulk MoS_2 (2θ = 14.4°, d = 0.614 nm), suggesting an enlarged interlayer distance of the (002) plane.[7,35] The distance is calculated to be 0.64 nm using the Bragg equation. This increased interlayer distance can provide desirable channels for Li ions intercalation with reduced diffusion barriers.[43−45]

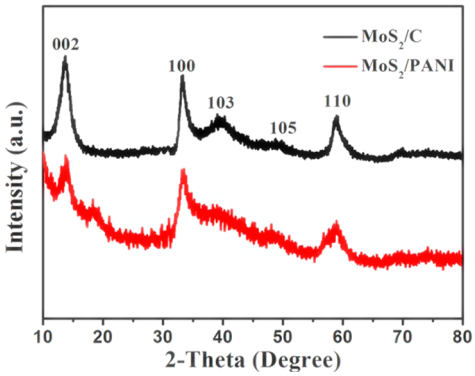

Figure 4. XRD patterns of the 3D hierarchical MoS_2/PANI and MoS_2/C nanoflowers.

X-ray photoelectron spectroscopy (XPS) was conducted to analyze the chemical states of Mo and S in the MoS_2/PANI and MoS_2/C samples (Figure 5). The Mo 3d XPS spectrum of MoS_2/PANI sample (Figure 5a) shows two broad peaks at 229 and 232.4 eV, which can be indexed as the doublet Mo $3d_{5/2}$ and Mo $3d_{3/2}$, respectively. A small S 2s peak is located at 226 eV. The peaks at 161.8 and 163.1 eV, corresponding to the S $2p_{3/2}$ and S $2p_{1/2}$ of divalent sulfide ions (S^{2-}), are observed in Figure 5b. These binding energies shown in Table S1 are in good agreement with those reported values for MoS_2 crystals.[46−48] For the MoS_2/C sample (Figure 5c and d), the Mo 3d spectrum shows two strong peaks almost at the same binding energies of 229.2 and 232.4 eV. However, the peaks corresponding to the S $2p_{3/2}$ and S $2p_{1/2}$ shift toward higher binding energies, indicating that electron transfer occurs in the hybrid structure of the MoS_2/C sample. So MoS_2 nanosheets are combined more tightly with the carbon matrix compared to PANI. It can be suggested that the outer electrons of S atom of MoS_2 interact with the carbon layer during the annealing process, and MoS_2 can be evenly embedded in the carbon matrix generating a hierarchical hybrid structure that have potential electronic conductivity.

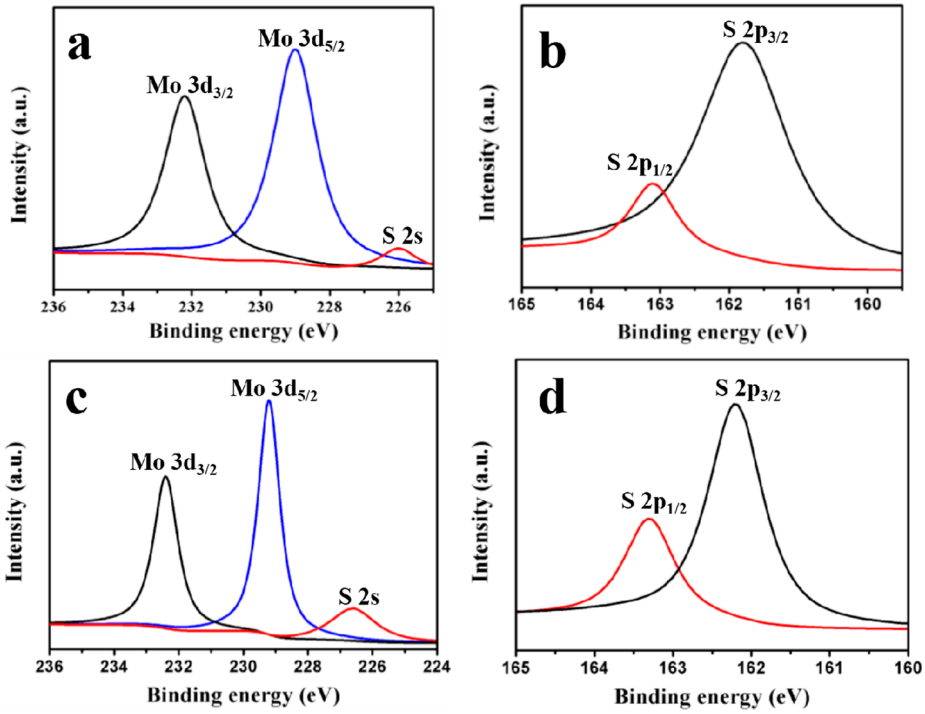

Figure 5. Mo 3d spectrum and S 2p spectrum taken from the 3D hierarchical MoS_2/PANI nanoflowers (a, b) and the MoS_2/C nanoflowers (c, d), respectively.

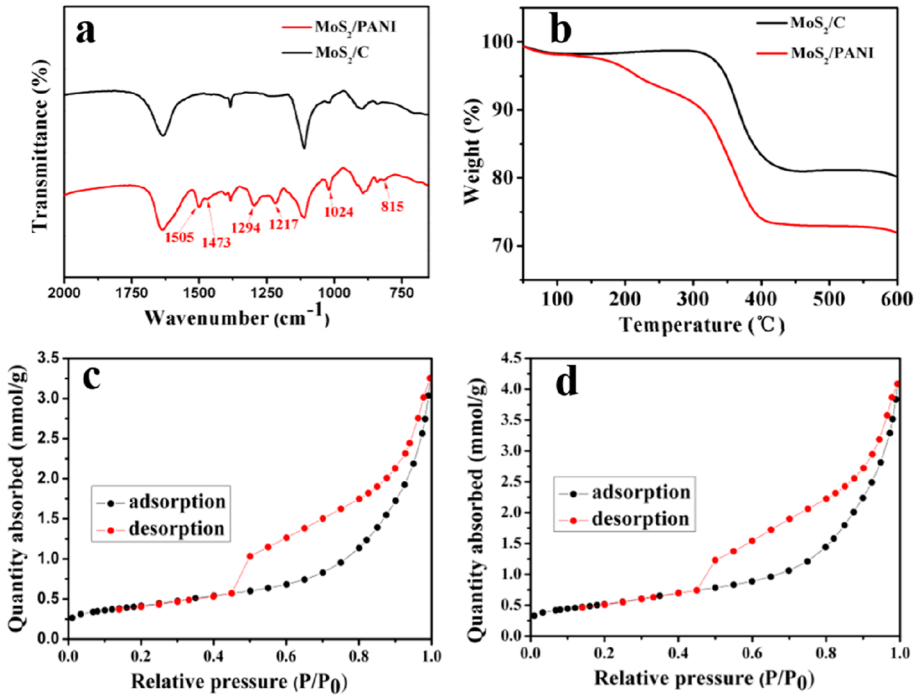

Figure 6. (a) FT-IR spectra and (b) TGA curves of the 3D hierarchical MoS_2/PANI and MoS_2/C nanoflowers. The N_2 adsorption−desorption isotherms of the 3D hierarchical MoS_2/PANI (c) and MoS_2/C (d) nanoflowers.

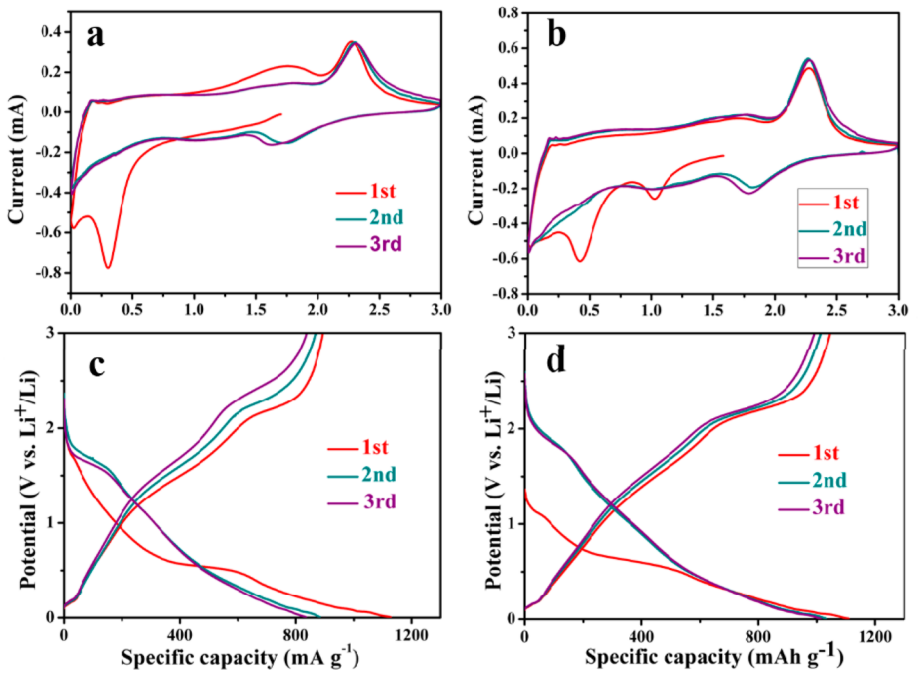

Figure 7. Cyclic voltammograms of the 3D hierarchical MoS_2/PANI (a) and MoS_2/C (b) nanoflowers for the first 3 cycles measured in the voltage range of 0−3.0 V with a scan rate of 0.1 mV s^{-1}. Voltage profiles of the 3D hierarchical MoS_2/PANI (c) and MoS_2/C (d) nanoflowers at a current density of 100 mA g^{-1}.

FT-IR spectroscopy was employed to confirm the composition of the two samples (Figure 6a). It is clear that the MoS_2/PANI sample exhibits the characteristic bands of PANI at 1505, 1473, 1294, 1217, 1124, and 815 cm^{-1}, revealing a PANI participant structure. Among these bands, 1505 and 1473 cm^{-1} are assigned to the C═C stretching of quinonoid (Q) and benzenoid (B) rings, 1294 and 1217 cm^{-1} belong to the C−N and C═N stretching of an aromatic amine, and 1124 and 815 cm^{-1} are associated with the bending of C−H in-plane and out-of-plane of aromatic ring.[49,50] On the other hand, the MoS_2/C sample shows no characteristic bands of PANI because of the carbonization of PANI. TGA was conducted to determine the amount of MoS_2 in the two samples (Figure 6b). Comparing the two TGA curves, we find that the MoS_2/PANI sample has a weight loss in the range of 160−300 °C, which can be attributed to the carbonization of PANI. With the

further increase of temperature, the two samples both have a significant weight loss in the range of 300−430 °C, which can be associated with the decomposition of amorphous carbon and the oxidation of MoS_2 to MoO_3. The mass fraction of MoS_2 in the MoS_2/PANI sample and the MoS_2/C sample can be calculated to be about 81% and 90%, respectively, assuming the final product after the TGA measurement is pure MoO_3. The nitrogen adsorption−desorption isotherms of the two samples are shown in Figure 6c and d. A typical hysteresis loop indicating a mesoporous structure is observed in both the MoS_2/PANI sample and the MoS_2/C sample. Both of them have a relatively high BET surface area of 33.0 and 41.3 $m^2\ g^{-1}$, respectively, resorting to the hierarchical flowerlike structures and the ultrathin dimension of nanoplates. The higher specific surface area of the MoS_2/C sample can be attributed to the effect of amorphous carbon.

The 3D hierarchical MoS_2/PANI and MoS_2/C nanoflowers are investigated as anode materials for LIBs. Figure 7a and b shows the first three cyclic voltammograms (CVs) of the MoS_2/PANI and MoS_2/C nanoflowers at a scan rate of 0.1 mV s^{-1}. In the first cathodic sweep, the MoS_2/PANI sample shows two peaks at around 1.5 and 0.3 V. While the MoS_2/C sample exhibits two distinct peaks locating at 1.1 and 0.4 V. The peak variation before and after annealing can be ascribed to the lithium intercalation on different defect sites of MoS_2. The peak at 1.5/1.1 V can be assigned to the formation of Li_xMoS_2 resulting from the intercalation of Li ions into MoS_2 layer, accompanying the phase transformation of MoS_2 from trigonal prismatic to octahedral coordination.[27,28] The peak at 0.3/0.4 V is related to the reduction of MoS_2 into Mo metal particles embedded into a Li_2S matrix and the formation of solid electrolyte interphase (SEI) film from electrochemically driven electrolyte degradation.[30−32] The overall reaction during this process can be described as $MoS_2 + 4Li^+ + 4e^- \rightarrow Mo + 2Li_2S$.[51] In the first anodic sweep of the MoS_2/PANI and MoS_2/C sample, the poorly defined peak located at about 1.78 V can be associated with the partial oxidation of Mo to MoS_2, and the following obvious peak at 2.27 V corresponds to the oxidation of Li_2S to S.[44,52] Thus, the electrode is mainly composed of Mo and S instead of the initial MoS_2 after the first cycle.[39] In the following cathodic sweeps, the peaks at 1.1 and 0.4 V disappear, and two new peaks at about 1.8 and 1.0 V emerge corresponding to the conversion of S to Li_2S and the association of Li with Mo,[53,54] respectively. Figure 7c and d shows the first three charge−discharge curves of the MoS_2/PANI sample and the MoS_2/C sample at a current density of 100 mA g^{-1} in the voltage range of 0.005−3 V. In the first discharge curve, two plateaus at approximately 1.65 and 0.6 V of the MoS_2/PANI sample and two plateaus at around 1.1 and 0.6 V of the MoS_2/C sample are observed, corresponding to the two lithiation processes of MoS_2.[55,56] In the second and third discharge curves of the MoS_2/PANI sample and the MoS_2/C sample, the plateau shown in the first curve disappears but two new plateaus at approximately 1.8 and 1.15 V emerge. In the charge curves, plateaus located at 1.7 and 2.2 V can be clearly defined. These results of the charge−discharge curves are in accordance with the aforementioned CVs. The initial lithiation (discharge) capacities of the MoS_2/PANI sample and the MoS_2/C sample are 1127 and 1109 mA h g^{-1}, with the corresponding delithiation (charge) capacities of 893 and 1043 mA h g^{-1}, resulting in high initial Coulombic efficiency of 79% and 94%, respectively. The higher Coulombic efficiency of MoS_2/C sample is attributed to more extracted lithium ions during the first charge process due to its excellent electronic conductivity, which is indicated by XPS experimental result.

The cycling performances of the MoS_2/PANI sample and MoS_2/C sample are shown in Figure 8a at a current density of

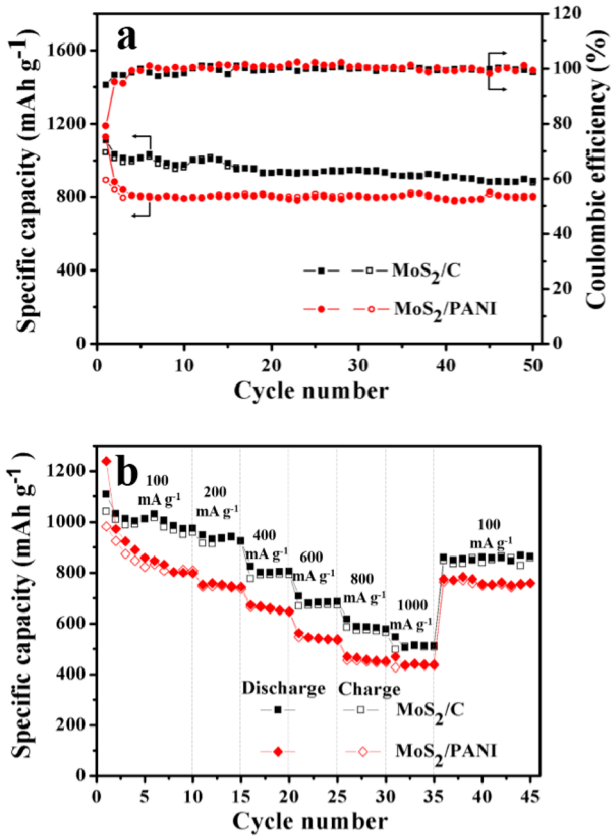

Figure 8. (a) Cycling performance and Coulombic efficiency of the 3D hierarchical MoS_2/PANI and MoS_2/C nanoflowers measured in the voltage range of 0.005−3.0 V at a current density of 100 mA g^{-1}. (b) Rate capability of the 3D hierarchical MoS_2/PANI and MoS_2/C nanoflowers between 0.005 and 3 V at different current densities.

100 mA g^{-1}. Notably, both the MoS_2/PANI sample and the MoS_2/C sample exhibit excellent cycling stability with high reversible specific capacities of 801.2 and 888.1 mAh g^{-1} after 50 cycles, respectively, which are much higher than that of pure MoS_2 (Figure S3, Supporting Information). The higher reversible capacity of the MoS_2/C sample can be attributed to the following three reasons: first, the MoS_2/C sample with larger specific surface area can provide enlarged contact area between the electrode material and electrolyte, thereby endowing it with more active sites for Li ion insertion/distraction. Second, the close integration of MoS_2 nanosheets with carbon matrix generating a hybrid nanostructure with higher charge mobility. Third, the content and the type of conductive material in the nanocomposite have great influence on the electrochemical performance, and the carbon with a mass fraction of 10% may be a more positive factor to the improvement of the electrochemical performance. Besides the high reversible capacities, the Coulombic efficiency of the MoS_2/PANI sample and the MoS_2/C sample are both maintained at above 95% from the second cycle. The rate capabilities of the MoS_2/PANI sample and the MoS_2/C sample are also evaluated as shown in Figure 8b. The MoS_2/C sample displays a better performance again. Specifically, the MoS_2/

PANI sample and the MoS_2/C sample deliver a reversible capacity of 798 and 975 mAh g^{-1}, respectively, at a current density of 100 mA g^{-1} after 10 cycles. When the current densities are increased, only a small decrease in capacity happened. A high reversible capacity of 439 mAh g^{-1} for the MoS_2/PANI sample and 511 mAh g^{-1} for the MoS_2/C sample can be achived even at a high current density of 1000 mA g^{-1} after 5 cycles. When the current density is changed back to 100 mA g^{-1}, the capacities of the MoS_2/PANI and the MoS_2/C sample can recover up to 758 and 863 mAh g^{-1} after 45 cycles at different current densities, revealing the good rate capability of the two samples.

EIS was conducted to further understand the excellent electrochemical performance of the MoS_2/PANI sample and the MoS_2/C sample (Figure 9a). The equivalent circuit model

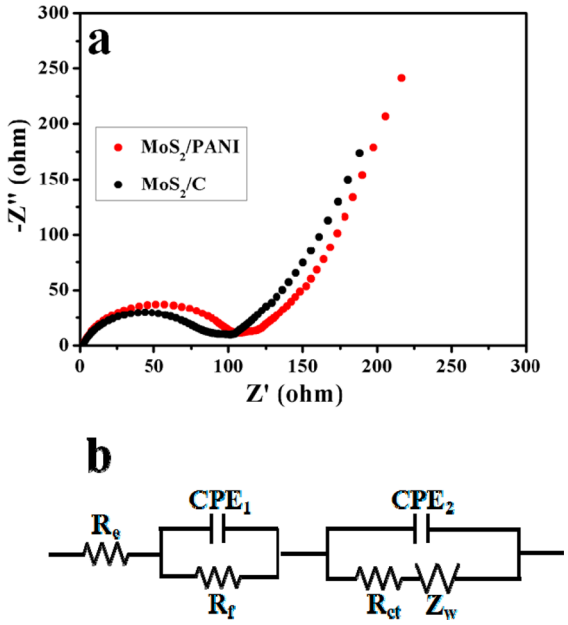

Figure 9. (a) Nyquist plots of the 3D hierarchical MoS_2/PANI and MoS_2/C nanoflowers tested in a frequency range of 0.01 Hz to 100 kHz. (b) Equivalent circuit model corresponding to the Nyquist plots of the 3D hierarchical MoS_2/PANI and MoS_2/C nanoflowers.

is also shown in Figure 9b to fit the Nyquist plots. The two curves shown in Figure 9a both consist of two semicircles at high and medium frequencies and an inclined line at low frequencies. According to previous reports,[28,57−59] the intercept on the Z' axis in the high-frequency region represents the resistance of the electrolyte (R_e); the high frequency semicircle can be assigned to the resistance R_f and CPE_1 of the SEI film; the medium frequency semicircle can be attributed to the charge transfer resistance R_{ct} and CPE_2 of the electrode/electrolyte interface; the inclined line is related with the Warburg impedance (Z_w) caused by the Li ions diffusion in the electrode materials. It can be seen that the semicircle of the MoS_2/C sample (Figure 9a) is smaller than that of the MoS_2/PANI sample, which contributes to the more excellent electrochemical performance of the MoS_2/C sample.

CONCLUSIONS

In summary, we have presented a simple method to synthesis 3D hierarchical MoS_2/PANI nanoflowers via a hydrothermal route and then annealing in a N_2 atmosphere at 500 °C for 4 h to further obtain the 3D hierarchical MoS_2/C nanoflowers. Structural characterizations show that the MoS_2/PANI and MoS_2/C nanoflowers are composed of ultrathin nanoplates, which consist of few-layered MoS_2 nanosheets with an expanded interlayer spacing and PANI or carbon. So the 3D hierarchical structures of the MoS_2/PANI and MoS_2/C nanoflowers both bring about relatively large specific area and sufficient void space between the neighboring nanoplates, which are beneficial to the great improvement of the electrochemical performance. According to the experimental test, the MoS_2/C nanoflowers exhibit more excellent electrochemical performance in virtue of the synergy of composition and novel hybrid nanostructure. So this reported method supplies a clue that can be generally extended to prepare more other active or conducive materials impregnated MoS_2 that owns ideal hierarchical structure. Further, through a simple annealing process, a 3D hierarchical MoS_2/C architecture can be built, which is an ideal candidate for application in LIBs.

ASSOCIATED CONTENT

Supporting Information

Photograph of PANI particles suspension obtained by dispersing the PANI in deionized water with the help of ultrasonication. TEM images of the annealed MoS_2 and the MoS_2/C nanoflowers. Cycling performanceof the MoS_2 and annealed MoS_2 measured in the voltage range of 0.005−3.0 V at a current density of 100 mA g^{-1}. Binding energies (BE) of elements in the 3D hierarchical MoS_2/PANI and MoS_2/C nanoflowers. This material is available free of charge via the Internet at http://pubs.acs.org.

AUTHOR INFORMATION

Corresponding Author

*E-mail: qunxu@zzu.edu.cn. Fax: +86 371 67767827. Tel: +86 371 67767827.

Notes

The authors declare no competing financial interest.

ACKNOWLEDGMENTS

We are grateful for the National Natural Science Foundation of China (No. 51173170, 21101141, 50955010, 20974102), the financial support from the Innovation Talents Award of Henan Province (114200510019), State Key Laboratory of Chemical Engineering (No. SKL-ChE-13A04), and the Key program of science and technology (121PZDGG213) from Zhengzhou Bureau of science and technology.

REFERENCES

(1) Goodenough, J. B.; Kim, Y. Challenges for Rechargeable Li Batteries. *Chem. Mater.* **2010**, *22*, 587−603.

(2) Choi, N. M.; Chen, Z.; Freunberger, S. A.; Ji, X.; Sun, Y. K.; Amine, K.; Yushin, G.; Nazar, L. F.; Cho, J.; Bruce, P. G. Challenges Facing Lithium Batteries and Electrical Double-Layer Capacitors. *Angew. Chem., Int. Ed.* **2012**, *51*, 9994−1002.

(3) Kang, D. H. P.; Chen, M. J.; Ogunseitan, O. A. Potential Environmental and Human Health Impacts of Rechargeable Lithium Batteries in Electronic Waste. *Environ. Sci. Technol.* **2013**, *47*, 5495−5503.

(4) Tarascon, J. M.; Armand, M. Issues and Challenges Facing Rechargeable Lithium Batteries. *Nature* **2001**, *414*, 359−367.

(5) Seo, J. W.; Jang, J. T.; Park, S. W.; Kim, C.; Park, B.; Cheon, J. Two-Dimensional SnS_2 Nanoplates with Extraordinary High Discharge Capacity for Lithium Ion Batteries. *Adv. Mater.* **2008**, *20*, 4269−4273.

(6) Zhai, C. X.; Du, N.; Zhang, H.; Yu, J. X.; Yang, D. R. Multiwalled Carbon Nanotubes Anchored with SnS_2 Nanosheets as High-Performance Anode Materials of Lithium-Ion Batteries. *ACS Appl. Mater. Interfaces* **2011**, *3*, 4067−4074.
(7) Du, G. D.; Guo, Z. P.; Guo, Z. P.; Wang, S. Q.; Zeng, R.; Chen, Z. X.; Liu, H. K. Superior Stability and High Capacity of Restacked Molybdenum Disulfide as Anode Material for Lithium Ion Batteries. *Chem. Commun.* **2010**, *46*, 1106−1108.
(8) Benavente, E.; Santa Ana, M. A.; Mendizabal, F.; Gonzalez, G. Intercalation Chemistry of Molybdenum Disulfide. *Chem. Rev.* **2002**, *224*, 87−109.
(9) Bhandavat, R.; David, L.; Singh, G. Synthesis of Surface-Functionalized WS_2 Nanosheets and Performance as Li-Ion Battery Anodes. *J. Phys. Chem. Lett.* **2012**, *3*, 1523−1530.
(10) Zhang, J.; Soon, J. M.; Loh, K. P.; Yin, J. H.; Ding, J.; Sullivian, M. B.; Wu, P. Magnetic Molybdenum Disulfide Nanosheet Films. *Nano Lett.* **2007**, *7*, 2370−2376.
(11) Wang, Q. H.; Kourosh, K. Z.; Kis, A.; Coleman, J. N.; Strano, M. S. Electronics and Optoelectronics of Two-Dimensional Transition Metal Dichalcogenides. *Nat. Nanotechnol.* **2012**, *7*, 699−712.
(12) Kan, M.; Wang, J. Y.; Li, X. W.; Zhang, S. H.; Li, Y. W.; Kawazoe, Y.; Sun, Q.; Jena, P. Structures and Phase Transition of a MoS_2 Monolayer. *J. Phys. Chem. C* **2014**, *118*, 1515−1522.
(13) Stephenson, T.; Li, Z.; Olsen, B.; Mitlin, D. Lithium Ion Battery Applications of Molybdenum Disulfide (MoS_2) Nanocomposites. *Energy Environ. Sci.* **2014**, *7*, 209−231.
(14) Sun, M.; Adjaye, J.; Nelson, A. E. Theoretical Investigations of the Structures and Properties of Molybdenum-Based Sulfide Catalysts. *Appl. Catal., A* **2004**, *263*, 131−143.
(15) Zhang, C.; Wang, Z.; Guo, Z.; Lou, X. W. Synthesis of MoS_2-C One-Dimensional Nanostructures with Improved Lithium Storage Properties. *ACS Appl. Mater. Interfaces* **2012**, *4*, 3765−3768.
(16) Zhou, X. S.; Wan, L. J.; Guo, Y. G. Synthesis of MoS_2 Nanosheet-Graphene Nanosheet Hybrid Materials for Stable Lithium Storage. *Chem. Commun.* **2013**, *49*, 1838−1840.
(17) Bindumadhavan, K.; Srivastava, S. K.; Mahanty, S. MoS_2-MWCNT Hybrids as a Superior Anode in Lithium-Ion Batteries. *Chem. Commun.* **2013**, *49*, 1823−1825.
(18) Zhou, X. S.; Wan, L. J.; Guo, Y. G. Facile Synthesis of MoS_2@CMK-3 Nanocomposite as an Improved Anode Material for Lithium-Ion Batteries. *Nanoscale* **2012**, *4*, 5868−5871.
(19) Li, H.; Li, W. J.; Ma, L.; Chen, W. X.; Wang, J. M. Electrochemical Lithiation/Delithiation Performances of 3D Flower-like MoS_2 Powders Prepared by Ionic Liquid Assisted Hydrothermal Route. *J. Alloys Compd.* **2009**, *471*, 442−447.
(20) Feng, Ch. Q.; Ma, J.; Li, H.; Zeng, R.; Guo, Z. P.; Liu, H. K. Synthesis of Molybdenum Disulfide (MoS_2) for Lithium Ion Battery Applications. *Mater. Res. Bull.* **2009**, *44*, 1811−1815.
(21) Ding, S.; Zhang, D.; Chen, J. S.; Lou, X. W. Facile Synthesis of Hierarchical MoS_2 Microspheres Composed of Few-layered Nanosheets and Their Lithium Ttorage Properties. *Nanoscale* **2012**, *4*, 95−98.
(22) Liang, S. Q.; Zhou, J.; Liu, J.; Pan, A. Q.; Tang, Y.; Chen, T.; Fang, G. Zh. PVP-Assisted Synthesis of MoS_2 Nanosheets With Improved Lithium Storage Properties. *CrystEngComm* **2013**, *15*, 4998−5002.
(23) Lu, C. X.; Liu, W. W.; Li, H.; Tay, B. K. A Binder-Free CNT Network-MoS_2 Composite as a High performance Anode Material in Lithium Ion Batteries. *Chem. Commun.* **2014**, *50*, 3338−3340.
(24) Park, S. K.; Yu, S. H.; Woo, S.; Quan, B.; Lee, D. Ch.; Kim, M. K.; Sung, Y. E.; Piao, Y. Z. A Simple L-Cysteine-Assisted Method for the Growth of MoS_2 Nanosheets on Carbon Nanotubes for High-Performance Lithium Ion Batteries. *Dalton Trans.* **2013**, *42*, 2399−2405.
(25) Ding, S.; Chen, J. S.; Lou, X. W. Glucose-Assisted Growth of MoS_2 Nanosheets on CNT Backbone for Improved Lithium Storage Properties. *Chem.—Eur. J.* **2011**, *17*, 13142−13145.
(26) Shi, Y. M.; Wang, Y.; Wong, J. I.; Tan, A. Y. Sh.; Hsu, Ch. L.; Li, L. J.; Lu, Y. Ch.; Yang, H. Y. Self-Assembly of Hierarchical MoS_x/CNT Nanocomposites ($2 < x < 3$): Towards High Performance Anode Materials for Lithium Ion Batteries. *Sci. Rep.* **2013**, *3*, 1−8.
(27) Zhao, J.; Lu, L.; Lotya, M.; Coleman, J. N.; Chou, Sh. L.; Liu, H. K.; Minett, A. I.; Chen, J. Development of MoS_2−CNT Composite Thin Film from Layered MoS_2 for Lithium Batteries. *Adv. Energy Mater.* **2013**, *6*, 798−805.
(28) Chang, K.; Chen, W. X. L-Cysteine-Assisted Synthesis of Layered MoS_2/Graphene Composites with Excellent Electrochemical Performances for Lithium Ion Batteries. *ACS Nano* **2011**, *5*, 4720−4728.
(29) Cao, X. H.; Shi, Y. M.; Shi, W. H.; Rui, X. H.; Yan, Q. Y.; Kong, J.; Zhang, H. Preparation of MoS_2-Coated Three-Dimensional Graphene Networks for High-Performance Anode Material in Lithium-Ion Batteries. *Small* **2013**, *9*, 3433−3438.
(30) Yu, H.; Ma, C.; Ge, B.; Chen, Y.; Xu, Z.; Zhu, C.; Li, C.; Ouyang, Q.; Gao, P.; Li, J.; Sun, C.; Qi, L.; Wang, Y.; Li, F. Three-Dimensional Hierarchical Architectures Constructed by Graphene/MoS_2 Nanoflake Arrays and Their Rapid Charging/Discharging Properties as Lithium-Ion Battery Anodes. *Chem.—Eur. J.* **2013**, *19*, 5818−5823.
(31) Gong, Y. J.; Yang, S. B.; Zhan, L.; Ma, L. L.; Vajtai, R.; Ajayan, P. M. A Bottom-Up Approach to Build 3D Architectures from Nanosheets for Superior Lithium Storage. *Adv. Funct. Mater.* **2014**, *24*, 125−130.
(32) Gong, Y.; Yang, S.; Liu, Z.; Ma, L.; Vajtai, R.; Ajayan, P. M. Graphene-Network-Backboned Architectures for High-Performance Lithium Storage. *Adv. Mater.* **2013**, *25*, 3979−3984.
(33) Chang, K.; Chen, W. In Situ Synthesis of MoS_2/Graphene Nanosheet Composites with Extraordinarily High Electrochemical Performance for Lithium Ion Batteries. *Chem. Commun.* **2011**, *47*, 4252−4254.
(34) Chang, K.; Chen, W. X.; Ma, L.; Li, H.; Huang, F. H.; Xu, Z. D.; Zhang, Q. B.; Lee, J. Y. Graphene-Like MoS_2/Amorphous Carbon Composites With High Capacity and Excellent Stability as Anode Materials for Lithium Ion Batteries. *J. Mater. Chem.* **2011**, *21*, 6251−6257.
(35) Fei, L.; Xu, Y.; Wu, X.; Chen, G.; Li, Y.; Li, B.; Deng, S.; Smirnov, S.; Fan, H.; Luo, H. Instant Gelation Synthesis of 3D Porous MoS_2@C Nanocomposites for Lithium Ion Batteries. *Nanoscale* **2014**, *6*, 3664−3669.
(36) Chang, K.; Chen, W. Single-Layer MoS_2/Graphene Dispersed in Amorphous Carbon: Towards High Electrochemical Performances in Rechargeable Lithium Ion Batteries. *J. Mater. Chem.* **2011**, *21*, 17175−17184.
(37) Zhang, L.; Lou, X. W. Hierarchical MoS_2 Shells Supported on Carbon Spheres for Highly Reversible Lithium Storage. *Chem.—Eur. J.* **2014**, *20*, 1−6.
(38) Wang, M.; Li, G. D.; Xu, H. Y.; Qian, Y. T.; Yang, J. Enhanced Lithium Storage Performances of Hierarchical Hollow MoS_2 Nanoparticles Assembled from Nanosheets. *ACS Appl. Mater. Interfaces* **2013**, *5*, 1003−1008.
(39) Yang, L. Ch.; Wang, S. N.; Mao, J. J.; Deng, J. W.; Gao, Q. Sh.; Tang, Y.; Schmidt, O. G. Hierarchical MoS_2/Polyaniline Nanowires with Excellent Electrochemical Performance for Lithium-Ion Batteries. *Adv. Mater.* **2013**, *25*, 1180−1184.
(40) Tian, Y.; He, Y.; Zhu, Y. F. Low Temperature Synthesis and Characterization of Molybdenum Disulfide Nanotubes and Nanorods. *Mater. Chem. Phys.* **2004**, *87*, 87−90.
(41) Sun, P.; Zhang, W.; Hu, X.; Yuan, L.; Huang, Y. Synthesis of Hierarchical MoS_2 and Its Electrochemical Performance as an Anode Material for Lithium-Ion Batteries. *J. Mater. Chem. A* **2014**, *2*, 3498−3504.
(42) Hu, S.; Chen, W.; Zhou, J.; Yin, F.; Uchaker, E.; Zhang, Q.; Cao, G. Preparation of Carbon Coated MoS_2 Flower-Like Nanostructure with Self-Assembled Nanosheets as High-Performance Lithium-Ion Battery Anodes. *J. Mater. Chem. A* **2014**, *2*, 7862−7872.
(43) Xiao, J.; Choi, D.; Cosimbescu, L.; Koech, P.; Liu, J.; Lemmon, J. P. Exfoliated MoS_2 Nanocomposite as an Anode Material for Lithium Ion Batteries. *Chem. Mater.* **2010**, *22*, 4522−4524.

(44) Hwang, H.; Kim, H.; Cho, J. MoS_2 Nanoplates Consisting of Disordered Graphene-like Layers for High Rate Lithium Battery Anode Materials. *Nano Lett.* **2011**, *11*, 4826−4830.
(45) Xie, J.; Zhang, H.; Li, S.; Wang, R.; Sun, X.; Zhou, M.; Zhou, J.; Lou, X. W. D.; Xie, Y. Defect-Rich MoS_2 Ultrathin Nanosheets with Additional Active Edge Sites for Enhanced Electrocatalytic Hydrogen Evolution. *Adv. Mater.* **2013**, *25*, 5807−5813.
(46) Liu, K. K.; Zhang, W.; Lee, Y. H.; Lin, Y. C.; Chang, M. T.; Su, C. Y.; Li, H.; Shi, Y.; Zhang, H.; Lai, C. S.; Li, L. J. Growth of Large-Area and Highly Crystalline MoS_2 Thin Layers on Insulating Substrates. *Nano Lett.* **2012**, *12*, 1538−1544.
(47) Altavilla, C.; Sarno, M.; Ciambelli, P. A Novel Wet Chemistry Approach for the Synthesis of Hybrid 2D Free-Floating Single or Multilayer Nanosheets of MS2@oleylamine (M = Mo, W). *Chem. Mater.* **2011**, *23*, 3879−3885.
(48) Chang, Y. H.; Lin, C. T.; Chen, T. Y.; Hsu, C. L.; Lee, Y. H.; Zhang, W.; Wei, K. H.; Li, L. J. Highly Efficient Electrocatalytic Hydrogen Production by MoS_x Grown on Graphene-Protected 3D Ni Foams. *Adv. Mater.* **2013**, *25*, 756−760.
(49) Chen, S. G.; Wei, Z. D.; Qi, X. Q.; Dong, L. C.; Guo, Y. G.; Wan, L. J.; Shao, Z. G.; Li, L. Nanostructured Polyaniline-Decorated Pt/C@PANI Core-Shell Catalyst with Enhanced Durability and Activity. *J. Am. Chem. Soc.* **2012**, *134*, 13252−13255.
(50) Zhang, K.; Zhang, L. L.; Zhao, X. S.; Wu, J. Graphene/Polyaniline Nanofiber Composites as Supercapacitor Electrodes. *Chem. Mater.* **2010**, *22*, 1392−1401.
(51) Fang, X. P.; Yu, X. Q.; Liao, S. F.; Shi, Y. F.; Hu, Y. S.; Wang, Z. X.; Stucky, G. D.; Chen, L. Q. Lithium Storage Performance in Ordered Mesoporous MoS_2 Electrode Material. *Microporous Mesoporous Mater.* **2012**, *151*, 418−423.
(52) Fang, X. P.; Guo, X. W.; Mao, Y.; Hua, C. X.; Shen, L. Y.; Hu, Y. S.; Wang, Z. X.; Wu, F.; Chen, L. Q. Mechanism of Lithium Storage in MoS_2 and the Feasibility of Using Li_2S/Mo Nanocomposites as Cathode Materials for Lithium-Sulfur Batteries. *Chem.—Asian J.* **2012**, *7*, 1013−1017.
(53) Xiao, J.; Wang, X.; Yang, X. Q.; Xun, S.; Liu, G.; Koech, P. K.; Liu, J.; Lemmon, J. P. Electrochemically Induced High Capacity Displacement Reaction of PEO/MoS_2/Graphene Nanocomposites with Lithium. *Adv. Funct. Mater.* **2011**, *21*, 2840−2846.
(54) Sen, U. K.; Mitra, S. High-Rate and High-Energy-Density Lithium-Ion Battery Anode Containing 2D MoS_2 Nanowall and Cellulose Binder. *ACS Appl. Mater. Interfaces* **2013**, *5*, 1240−1247.
(55) Wang, Z.; Ma, L.; Chen, W.; Huang, G.; Chen, D.; Wang, L.; Lee, J. Y. Facile Synthesis of MoS_2/Graphene Composites: Effects of Different Cationic Surfactants on Microstructures and Electrochemical Properties of Reversible Lithium Storage. *RSC Adv.* **2013**, *3*, 21675−21684.
(56) Huang, G.; Chen, T.; Chen, W.; Wang, Z.; Chang, K.; Ma, L.; Huang, F.; Chen, D.; Lee, J. Y. Graphene-like MoS_2/Graphene Composites: Cationic Surfactant-Assisted Hydrothermal Synthesis and Electrochemical Reversible Storage of Lithium. *Small* **2013**, *9*, 3693−3703.
(57) Wang, Ch.; Wan, W.; Huang, Y. H.; Chen, J. T.; Zhou, H. H.; Zhang, X. X. Hierarchical MoS_2 Nanosheets/Active Carbon Fiber Cloth as Binder-Free and Free-Standing Anodes for Lithium-Ion Batteries. *Nanoscale* **2014**, *6*, 5351−5358.
(58) Zhao, C.; Kong, J.; Yao, X.; Tang, X.; Dong, Y.; Phua, S. L.; Lu, X. Thin MoS_2 Nanoflakes Encapsulated in Carbon Nanofibers as High-Performance Anodes for Lithium-Ion Batteries. *ACS Appl. Mater. Interfaces* **2014**, *6*, 6392−6398.
(59) Wang, Z.; Chen, T.; Chen, W. X.; Chang, K.; Ma, L.; Huang, G. C.; Chen, D. Y.; Lee, J. Y. CTAB-Assisted Synthesis of Single-Layer MoS_2-Graphene Composites as Anode Materials of Li-Ion Batteries. *J. Mater. Chem. A* **2013**, *1*, 2202−2210.